Analysis of Transcranial Magnetic Stimulation Based on the Surface Integral Equation Formulation

Mario Cvetković*, *Student Member, IEEE*, Dragan Poljak, *Senior Member, IEEE*, and Jens Haueisen, *Member, IEEE*

***Abstract*— *Goal:* The aim of this paper is to provide a rigorous model and, hence, a more accurate description of the transcranial magnetic stimulation (TMS) induced fields and currents, respectively, by taking into account the inductive and capacitive effects, as well as the propagation effects, often being neglected when using quasi-static approximation. *Methods:* The formulation is based on the surface integral equation (SIE) approach. The model of a lossy homogeneous brain has been derived from the equivalence theorem and using the appropriate boundary conditions for the electric field. The numerical solution of the SIE has been carried out using the method of moments. *Results:* Numerical results for the induced electric field, electric current density, and the magnetic flux density distribution inside the human brain, presented for three typical TMS coils, are in a good agreement with some previous analysis as well as to the results obtained by analytical approach. *Conclusion:* The future work should be related to the development of a more detailed geometrical model of the human brain that will take into account complex cortical columnar structures, as well as some additional brain tissues. *Significance:* To the best of authors knowledge, similar approach in modeling TMS has not been previously reported, albeit integral equation methods are seeing a revival in computational electromagnetics community.**

***Index Terms*—Electromagnetic model, numerical solution, surface integral equation (SIE) approach, transcranial magnetic stimulation (TMS).**

I. Introduction

TRANSCRANIAL magnetic stimulation (TMS) is a noninvasive and painless technique for stimulation or inhibition of certain brain regions. A stimulation coil placed near the surface of a patient's head is energized by a very short current pulse, generating the time-varying magnetic field of high intensity penetrating into nearby tissues such as skull and brain. According to the differential form of Faraday's law, the time-varying magnetic field induces an electric field, thus depolarizing or hyperpolarizing the neuronal cell membranes located within a few centimeters of the cortex. When the membrane potential reaches certain threshold value, the action potential is generated. Macroscopically, brain activation occurs in the regions with the highest values of the induced electric field [1]–[4].

Manuscript received April 4, 2014; revised January 9, 2015; accepted January 10, 2015. Date of publication January 16, 2015; date of current version May 18, 2015. *Asterisk indicates corresponding author.*

*M. Cvetković is with the Faculty of Electrical Engineering, Mechanical Engineering, and Naval Architecture, University of Split, 21000 Split, Croatia (e-mail: mcvetkov@fesb.hr).

D. Poljak is with the Faculty of Electrical Engineering, Mechanical Engineering, and Naval Architecture, University of Split.

J. Haueisen is with the Institute of Biomedical Engineering and Informatics, Ilmenau University of Technology, and the Biomagnetic Centre, Jena University Hospital.

Color versions of one or more of the figures in this paper are available online at http://ieeexplore.ieee.org.

Digital Object Identifier 10.1109/TBME.2015.2393557

Although the technology necessary for the TMS development has been known for some time, the technique obtained a huge impetus in 1985, today considered as the birth year of TMS, when Barker *et al.* [5] from the University of Sheffield demonstrated the first stimulation of spinal cord having also arrived to the idea of direct and noninvasive stimulation of brain. From those days on, the basic technique for magnetic stimulation practically has remained almost the same. A few years later, the group led by Ueno showed [6], [7] that the localized stimulation of the brain could be achieved by using a pair of coils, thus the figure-of-eight coil (8-coil) was introduced.

During the following thirty years, TMS has become a valuable tool in not only the study of specific cortex areas but also in diagnostics and for therapeutic purposes. In addition to the treatment of depression, which is so far the most commonly studied application of TMS, this technique can be applied in various other neurological and psychiatric disorders.

Although TMS is a widely used technique, much more research is needed on the distribution of the electromagnetic fields induced in the human brain. Modeling of brain stimulation is important for determining the exact location and the level of stimulation, as well as to clarify the related underlying mechanisms. The modeling is also helpful in the interpretation of the experimental results and in the design of a new, more efficient stimulation systems, such as multicoil designs for focused and deep brain stimulation [8]–[10].

There were many attempts to develop brain models, varying in complexity from homogeneous spherical ones [11], [12], to a more recent realistic three-dimensional (3-D) models using a number of various tissues [13]–[15].

The advantage of simple canonical models is the available analytical solution [11], [16], thus making them useful for initial assessment of the distribution of the induced field. For more realistic representations, the solution can be attained using numerical methods.

Regarding the formulation of the problem, there are approaches based on the differential and integral equation, respectively. From the early days, the differential approach has become the *method of choice* in the mathematical formulation of the problems related to the determination of induced electric fields inside biological tissues, and TMS modeling is no exception.

One of the drawbacks of the differential equation approach is a need for the entire domain discretization. In case of an open boundary problems, such as radiation and scattering, one needs to artificially limit the boundary of the problem or use concepts such as infinite elements, absorbing boundary conditions, etc. On the other hand, integral equation-based formulations require only discretization of the boundary, allowing an additional

benefit of reducing the dimensionality of the problem. Furthermore, since boundary conditions are implicit within the integral formulation, open boundary problems are treated in an exact way.

In recent decades, integral equation-based approach is seeing a revival in computational electromagnetics community [17]. There is some reported work where the TMS problem is treated by the boundary element method [14], [18]. Nevertheless, an application of surface integral equation (SIE) analysis methods to TMS has not been reported in the relevant available literature. The development of a rigorous TMS model using the integral equations would, thus, provide a means for an alternative more accurate physical description of the problem.

Since electromagnetic fields related to TMS are of low frequency, the so called *quasi-static approximation* is frequently used. Under quasi-static approximation, usually some of the assumptions are adopted, usually these being either the neglection of the inductive or the capacitive effects, as well as the propagation effects, thus allowing simplification of the expressions used for determining induced field and currents. Although the approximation is valid for low frequencies, as originally formulated in [19], the frequency spectrum of modern stimulators frequently exceeds 1 kHz.

Many authors eventually showed that the approximation is inappropriate at higher frequencies, i.e., propagation effects at very high values [20] of tissues permittivity [21], [22], as well as capacitive effects [23] are no longer negligible, and their exclusion could lead to an incorrect determination of the stimulated area [24]–[26].

Nevertheless, the majority of the present methods use quasi-static approximation in determining the distribution of TMS induced electric fields and electric currents in the human brain [6], [11], [13]–[16], [20], [27]–[33].

This paper presents a rigorous integral equation-based model of TMS that will enable a more accurate physical description of the problem, thus, avoiding the use of quasi-static approximation. This paper is organized as follows: Derivation of an electromagnetic model using the equivalence theorem and appropriate boundary conditions is carried out in the first part. Furthermore, the numerical method based on the scheme of method of moments (MoMs) is presented, followed by the related numerical solution of the coupled set of electric field integral equations (EFIEs). The numerical results obtained via the proposed model are presented for three typical TMS coils. The final part of this paper gives a brief discussion and a conclusion containing some suggestions for a future work. This paper could be viewed as an opener to the subject regarding the integral equation-based approach in modeling bioelectromagnetics phenomena.

II. Methods

A. Formulation

If the problem of the human brain exposed to TMS coil is approached as a classical scattering problem, the equivalence theorem and the appropriate boundary conditions for the electric and/or magnetic field can be used for derivation of the electromagnetic model based on the SIE.

To apply the equivalence theorem, the human brain is first replaced by an arbitrarily-shaped dielectric body S of a homogeneous properties (ε_1, μ_1), placed in free space, as shown in Fig. 1(a).

As the present study represents the first implementation of the proposed model, to facilitate the solution process, we consider a brain compartment model only and neglect the skull and scalp because the majority of the current is flowing inside the skull [34].

To account for inductive and capacitive effects, the brain is considered as a lossy material with complex permittivity and permeability (ε_2, μ_2). Due to the fact that biological tissues do not possess magnetic properties, the value for the permeability of the brain is taken to be μ_0, i.e., the free space permeability, while the complex permittivity of the brain is given by

$$\varepsilon_2 = \varepsilon_0 \varepsilon_r - j\frac{\sigma}{\omega} \tag{1}$$

where ε_0 is the permittivity of the free space, ε_r is the relative permittivity, σ is the electrical conductivity of the brain, and $\omega = 2\pi f$ is the operating frequency.

The electromagnetic field $(\vec{E}^{\text{inc}}, \vec{H}^{\text{inc}})$ is incident on the lossy homogeneous object representing the brain. Due to the presence of the scattering object, i.e., brain, a scattered field denoted by $(\vec{E}^{\text{sca}}, \vec{H}^{\text{sca}})$ is also present. The fields exterior and interior to the surface S of the object are $(\vec{E}_1, \vec{H}_1)$ and $(\vec{E}_2, \vec{H}_2)$, respectively. Also, on the surface S, unit vector $\hat{n}$ is placed, pointing from region 2 into region 1, as seen in Fig. 1.

Applying the equivalence theorem for regions 1 and 2, two equivalent problems can be formulated, in terms of the equivalent electric and magnetic current densities $\vec{J}$ and $\vec{M}$ placed on the surface S [17], [35]–[37]. These equivalent problems are shown in Fig. 1(b) and (c), for the external and internal region, respectively.

In the case of an external equivalent problem, shown in Fig. 1(b), the field inside is assumed to be zero, $(\vec{E}_2 = 0, \vec{H}_2 = 0)$, so that material properties of this region could be chosen arbitrarily. Selecting the same properties as that of an exterior region, leads to the homogeneous domain of (ε_1, μ_1), allowing one to use the Green's function for free space. To satisfy the boundary conditions on the surface S, equivalent surface currents $\vec{J}_1$ and $\vec{M}_1$ are introduced at this surface. Following the same procedure for the interior equivalent problem, another homogeneous domain with properties (ε_2, μ_2) is obtained. Again, the equivalent surface currents $\vec{J}_2 = -\vec{J}_1$ and $\vec{M}_2 = -\vec{M}_1$ are introduced to the surface S, as indicated in Fig. 1(c).

Since the obtained equivalent problems represent equivalent current densities radiating in a homogeneous medium, the following expressions for the scattered fields due to these sources can be used

$$\vec{E}_i^{\text{sca}}(\vec{J}, \vec{M}) = -j\omega\vec{A}_i - \nabla\varphi_i - \frac{1}{\varepsilon_i}\nabla \times \vec{F}_i \tag{2}$$

$$\vec{H}_i^{\text{sca}}(\vec{J}, \vec{M}) = -j\omega\vec{F}_i - \nabla\psi_i + \frac{1}{\mu_i}\nabla \times \vec{A}_i \tag{3}$$

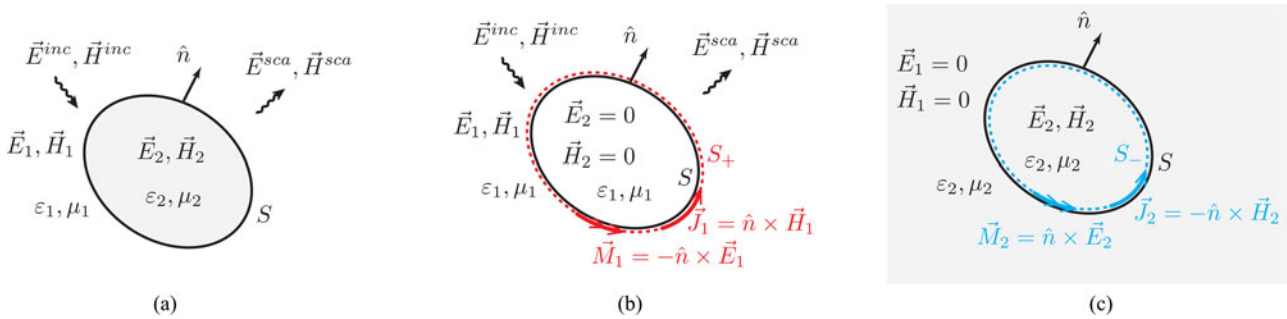

Fig. 1. Human brain as a lossy homogeneous dielectric (ε_2, μ_2) placed in the incident field $(\vec{E}^{\rm inc}, \vec{H}^{\rm inc})$ of a TMS coil. (a) Original problem, (b) Equivalent problem for region 1. (c) Equivalent problem for region 2.

where the index $i = 1, 2$ denotes medium where equivalent surface currents radiate, and φ, $\vec{F}$, ψ, and $\vec{A}$ are scalar and vector, electric and magnetic potentials, respectively.

These potentials are given in terms of surface integrals over the sources, i.e.,

$$\vec{A}_i(\vec{r}) = \mu_i \iint_S \vec{J}(\vec{r}\,')G_i(\vec{r}, \vec{r}\,')\,\mathrm{d}S' \tag{4}$$

$$\vec{F}_i(\vec{r}) = \varepsilon_i \iint_S \vec{M}(\vec{r}\,')G_i(\vec{r}, \vec{r}\,')\,\mathrm{d}S' \tag{5}$$

$$\varphi_i(\vec{r}) = \frac{1}{\varepsilon_i} \iint_S \rho(\vec{r}\,')G_n(\vec{r}, \vec{r}\,')\,\mathrm{d}S' \tag{6}$$

$$\psi_i(\vec{r}) = \frac{1}{\mu_i} \iint_S m(\vec{r}\,')G_n(\vec{r}, \vec{r}\,')\,\mathrm{d}S' \tag{7}$$

where ρ and m are the electric and magnetic charge density, respectively, and $G_i(\vec{r}, \vec{r}\,')$ is the Green's function for the homogeneous medium i given by

$$G_i(\vec{r}, \vec{r}\,') = \frac{e^{-jk_iR}}{4\pi R}; \quad R = |\vec{r} - \vec{r}\,'|. \tag{8}$$

In (8), R is the distance from the observation point $\vec{r}$ to the source point $\vec{r}\,'$, and $k_i = \omega\sqrt{\mu_i\varepsilon_i}$ is a wave number of a medium i.

Using (4)–(7), the scattered field from (2) and (3) can be expressed in terms of the equivalent surface currents. Applying the boundary conditions at the surface S being interface of the two equivalent problems, a set of four equations for the electric and magnetic field, respectively, is obtained. Choosing two expressions for the electric field

$$-\hat{n} \times \vec{E}_i^{\rm sca}(\vec{J}, \vec{M}) = \begin{cases} \hat{n} \times \vec{E}^{\rm inc}, & i = 1 \\ 0, & i = 2 \end{cases} \tag{9}$$

the EFIE formulation in the frequency domain for the lossy homogeneous human brain is obtained. In (9), $\vec{E}^{\rm inc}$ is the known incident field, e.g., generated by a TMS coil, while $\vec{J}$ and $\vec{M}$ represent unknown surface currents.

Using the continuity equation, the electric and magnetic charge in (6) and (7) can be replaced with the divergence of the electric and magnetic current, respectively, and after inserting (4)–(7) in (2), the set of coupled integral equations is obtained

$$\begin{aligned} & j\omega\mu_i \iint_S \vec{J}(\vec{r}\,')G_i(\vec{r}, \vec{r}\,')\,\mathrm{d}S' \\ & -\frac{j}{\omega\varepsilon_i}\nabla \iint_S \nabla'_S \cdot \vec{J}(\vec{r}\,')G_i(\vec{r}, \vec{r}\,')\,\mathrm{d}S' \\ & +\nabla \times \iint_S \vec{M}(\vec{r}\,')G_i(\vec{r}, \vec{r}\,')\,\mathrm{d}S' = \begin{cases} \vec{E}^{\rm inc}, & i = 1 \\ 0, & i = 2. \end{cases} \end{aligned} \tag{10}$$

Performing certain mathematical manipulations on the second and third integral of (10), the nabla operator can be transferred to the Green's function, leading to

$$\begin{aligned} & j\omega\mu_i \iint_S \vec{J}(\vec{r}\,')G_i(\vec{r}, \vec{r}\,')\,\mathrm{d}S' \\ & -\frac{j}{\omega\varepsilon_i} \iint_S \nabla'_S \cdot \vec{J}(\vec{r}\,')\nabla G_i(\vec{r}, \vec{r}\,')\,\mathrm{d}S' \\ & + \iint_S \vec{M}(\vec{r}\,') \times \nabla' G_i(\vec{r}, \vec{r}\,')\,\mathrm{d}S' = \begin{cases} \vec{E}^{\rm inc}, & i = 1 \\ 0, & i = 2. \end{cases} \end{aligned} \tag{11}$$

Details of the above procedure can be found in Appendix A.

B. Numerical Solution

The set of coupled integral (11) cannot be solved analytically for a complex geometry of the surface S, therefore a numerical approach must be used. This paper features the use of the MoM. The unknown currents are expanded by

$$\vec{J}(\vec{r}) = \sum_{n=1}^{N} J_n \vec{f}_n(\vec{r}) \tag{12}$$

$$\vec{M}(\vec{r}) = \sum_{n=1}^{N} M_n \vec{g}_n(\vec{r}) \tag{13}$$

where J_n and M_n are unknown coefficients, $\vec{f}_n$ and $\vec{g}_n$ are known expansion or basis functions, and N stands for the total number of elements used in the discretization of surface S.

C. Human Brain Model

The brain model was generated from a freely available Google Sketchup rendering of the human brain, as shown on Fig. 2(a).

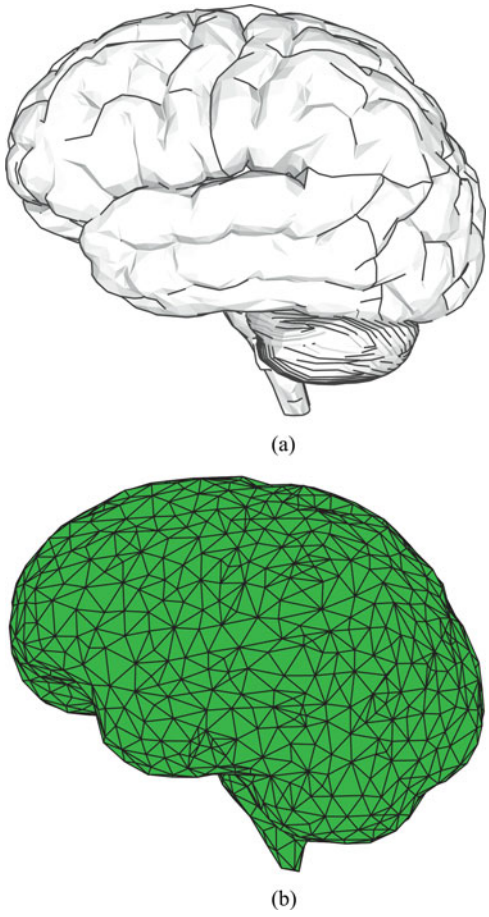

Fig. 2. Human brain model for SIE formulation. (a) Detailed 3-D model from Google Sketchup. (b) Final model discretized using the triangular elements imported into MATLAB.

Dimensions of the brain are: Length: 167 mm, width: 140 mm, height: 93 mm, and volume: 1400 cm^3 [38].

The brain model is imported into an open source program called MeshLab [39] where meshing using the triangular elements has been performed. The brain surface is discretized using the $T = 696$ triangular elements and $N = 1044$ edge-elements. The final model, shown in Fig. 2(b), was imported into MATLAB where the processing part has been carried out.

D. Expansion of Surface Currents

Triangular discretization of the brain surface enables one to use the so called Rao–Wilton–Glisson (RWG) expansion function [40] in (12) and (13). The RWG function $\vec{f}_n$ is defined on a pair of triangles T_n^+ and T_n^- sharing a common edge (hence, sometimes called edge element), while the function vanishes on the rest of the surface S. The function is given by

$$\vec{f}_n^{\pm}(\vec{r}) = \begin{cases} \dfrac{l_n}{2A_n^{\pm}}\vec{\rho}_n^{\pm}, & \vec{r} \in T_n^{\pm} \\ 0, & \vec{r} \notin T_n^{\pm} \end{cases} \tag{14}$$

where l_n is the length at the interface of triangles T_n^+ and T_n^-, while A_n^+ and A_n^- are the surface areas of those triangles. The vector $\vec{\rho}_n^+ = \vec{r} - \vec{r}_n^+$ is directed from the free vertex of T_n^+ and $\vec{\rho}_n^- = \vec{r}_n^- - \vec{r}$ is directed to the free vertex of T_n^-.

The surface electric current $\vec{J}$ is approximated by the RWG function $\vec{f}_n$, while the surface magnetic current $\vec{M}$ is approximated by the pointwise orthogonal function $\vec{g}_n$, where

$$\vec{g}_n = \hat{n} \times \vec{f}_n. \tag{15}$$

Using (14) and (15), the unknown equivalent currents $\vec{J}(\vec{r}')$ and $\vec{M}(\vec{r}')$ from (11) can be approximated by (12) and (13). Multiplying (11) by the set of a test functions $\vec{f}_m$, where $\vec{f}_m = \vec{f}_n$, and integrating over surface S, followed by a rather demanding procedure described in more details in Appendix B, yields

$$\begin{aligned} & j\omega\mu_i \sum_{n=1}^{N} J_n \iint_S \vec{f}_m(\vec{r}) \cdot \iint_{S'} \vec{f}_n(\vec{r}')G_i \, dS' \, dS \\ & + \frac{j}{\omega\varepsilon_i} \sum_{n=1}^{N} J_n \iint_S \nabla_S \cdot \vec{f}_m(\vec{r}) \iint_{S'} \nabla'_S \cdot \vec{f}_n(\vec{r}')G_i \, dS' dS \\ & + \sum_{n=1}^{N} M_n \iint_S \vec{f}_m(\vec{r}) \cdot [\hat{n} \times \vec{g}_n(\vec{r}')] \, dS \\ & + \sum_{n=1}^{N} M_n \iint_S \vec{f}_m(\vec{r}) \cdot \iint_{S'} \vec{g}_n(\vec{r}') \times \nabla' G_i \, dS' \, dS \\ & = \begin{cases} \iint_S \vec{f}_m(\vec{r}) \cdot \vec{E}^{\text{inc}} \, dS, & i = 1 \\ 0, & i = 2 \end{cases} \end{aligned} \tag{16}$$

where the subscript i is index of the medium, $i = 1, 2$. Extracting two sums, (16) can be written as the following system of linear equations

$$\begin{aligned} & \sum_{n=1}^{N} \left(j\omega\mu_i A_{mn,i} + \frac{j}{\omega\varepsilon_i} B_{mn,i} \right) J_n \\ & + \sum_{n=1}^{N} \left(C_{mn,i} + D_{mn,i} \right) M_n = \begin{cases} V_m, & i = 1 \\ 0, & i = 2. \end{cases} \end{aligned} \tag{17}$$

Expression (17) can be written in the compact matrix form

$$[\mathbf{Z}] \cdot \{\mathbf{I}\} = \{\mathbf{V}\} \tag{18}$$

where $\mathbf{Z}$ represents the $2N \times 2N$ matrix of a system, while $\mathbf{V}$ is the source vector of a dimension $2N$.

The vector $\mathbf{I}$ containing the unknown coefficients J_n and M_n is the solution of the matrix (18). From these coefficients, the equivalent electric and magnetic currents $\vec{J}$ and $\vec{M}$ placed on the surface S of the dielectric object, i.e., the human brain, can be determined using (12) and (13). Obtaining these currents, the electric and magnetic field can be easily determined at arbitrary

points in brain, using

$$\begin{aligned}\vec{E}_2(\vec{r}) = & -j\omega\mu_2 \iint_S \vec{J}(\vec{r}\,')G_2(\vec{r},\vec{r}\,')\,dS' \\ & - \frac{j}{\omega\varepsilon_2}\iint_S \nabla'_S \cdot \vec{J}(\vec{r}\,')G_2(\vec{r},\vec{r}\,')\,dS' \\ & - \iint_S \vec{M}(\vec{r}\,') \times \nabla G_2(\vec{r},\vec{r}\,')\,dS' \end{aligned} \tag{19}$$

and

$$\begin{aligned}\vec{H}_2(\vec{r}) = & -j\omega\varepsilon_2 \iint_S \vec{M}(\vec{r}\,')G_2(\vec{r},\vec{r}\,')\,dS' \\ & - \frac{j}{\omega\mu_2}\iint_S \nabla'_s \cdot \vec{M}(\vec{r}\,')G_2(\vec{r},\vec{r}\,')\,dS' \\ & + \iint_S \vec{J}(\vec{r}\,') \times \nabla' G_2(\vec{r},\vec{r}\,')\,dS' \end{aligned} \tag{20}$$

respectively.

E. Field of a TMS Coil

The incident electric field $\vec{E}_{\rm inc}$ from (9) is due to some external sources, and exists regardless of the presence of a dielectric object, i.e., the brain. Usually, for the case of a plane-wave incidence, these sources are placed at infinity. On the other hand, TMS coil placed in the vicinity of the head can be considered as a near field source, hence posing a coupled problem. Consequently, the induced eddy currents in the brain will in turn generate a secondary field superimposed to the primary field due to coil current.

The electric field due to TMS can be expressed as follows:

$$\vec{E} = -j\omega\vec{A} - \nabla\varphi \tag{21}$$

where $\vec{A}$ and φ are the magnetic vector potential and electric scalar potential, respectively. The first term in (21) is due to current flowing in the coil, while the second one is the consequence of the accumulation of electric charge on the boundary of the medium [41]. If TMS coil is placed in free space, the second term in (21) is zero, hence, the electric field due to coil can be calculated from

$$\vec{E} = -j\omega\vec{A}. \tag{22}$$

Assuming a uniform current density I over a coil cross section, magnetic vector potential at an arbitrary point can be determined from integral

$$\vec{A}(\vec{r}) = \frac{\mu_0 MI}{4\pi}\int_l \frac{d\vec{l}}{|\vec{r}-\vec{r}\,'|} \tag{23}$$

where μ_0 is the free space permeability, M is the number of coil windings, and $|\vec{r}-\vec{r}\,'|$ is the distance from the observation to the source point on the coil. The differential element of the curve $d\vec{l}$ depicts the direction of the current flow through the coil. Expression (23) can be solved by discretizing the coil with linear segments [42]. Assembling the contributions from all linear segments, the magnetic vector potential can be determined at an arbitrary point in space.

TABLE I
HOMOGENEOUS HUMAN BRAIN PARAMETERS, FROM [43]

Frequency	
2.44 kHz	
Relative permittivity [-]	Electrical conductivity [S/m]
ε_r	σ
46 940	0.08595

On the other hand, the magnetic flux density $\vec{B}$ at an arbitrary point in space can be determined from the Biot–Savart's law

$$\vec{B}(\vec{r}) = \frac{\mu_0 MI}{4\pi}\int_l \frac{d\vec{l}\times\hat{r}_0}{|\vec{r}-\vec{r}\,'|^3} \tag{24}$$

where $\hat{r}_0$ is the unit vector pointing from the source point $\vec{r}\,'$ to the field point $\vec{r}$. It should be noted that, due to the simple form, (21) and (24) often serve as the first estimation of TMS coil induced electric field and the magnetic flux density. In this paper, expressions (21)–(24) are used only for comparison purposes to the results obtained using a rigorous approach. In this paper, the term involving incident field (due to TMS coil) is calculated under the assumption that the coil is placed in free space. It should be noted that the coil description via linear approximation is not a novelty itself.

F. Calculation of the Induced Field and Current Density

In the presented model, (22) with (23) are used only to determine the incident field $\vec{E}_{\rm inc}$ generated by the TMS coil, which serves as the input data for the SIE formulation (11). By using these expressions, the TMS coil is assumed to be decoupled from the human brain, i.e., its presence does not disturb the field.

The electric and magnetic field, generated by the induced equivalent surface currents itself, at an arbitrary point inside the brain are calculated using (19) and (20), respectively. The magnetic flux density in the brain is calculated from

$$\vec{B} = \mu_0\vec{H}. \tag{25}$$

From the field $\vec{E}$ inside the brain, the distribution of the current density $\vec{J}_{\rm ind}$ for the lossy homogeneous brain is determined by

$$\vec{J}_{\rm ind} = (\sigma + j\omega\varepsilon_0\varepsilon_r)\,\vec{E} \tag{26}$$

where σ and ε_r are the electric conductivity and relative permittivity of the human brain, respectively. Frequency-dependent parameters of the homogeneous brain tissue, given in Table I, were taken from database [43], [44], as an average of white matter (WM) and gray matter (GM).

The literature values for brain conductivity vary largely. While the value for CSF is relatively well known [45], the values for white and gray matter for low frequencies have been reported between 0.01 and 1 S/m [46]. The specific conductivity value chosen for this study is well within this range. In future studies, we plan to investigate the influence of different conductivity values in a three compartment head model.

TABLE II
COIL PARAMETERS

	Circular	8-coil	Butterfly
Frequency	2.44 kHz	2.44 kHz	2.44 kHz
Radius of turn	4.5 cm	3.5 cm	3.5 cm
No. of turns	14	15	15
Coil current	2843 A	2843 A	2843 A

TABLE III
COMPARISON OF MAXIMUM ELECTRIC FIELD OBTAINED VIA ANALYTICAL EXPRESSION AND VIA PROPOSED MODEL

		Circular	8-coil	Butterfly
Analytical				
E_{max}	[V/m]	161.15	321.94	328.01
Proposed SIE model				
E_{max}	[V/m]	86.83	118.28	138.41

III. NUMERICAL RESULTS

The computational examples are based on the three generic coils used in TMS, namely, the standard circular coil, the 8-coil, and the butterfly coil (8-coil with wings inclined at 10°). The circular coil is discretized into 80 linear segments, the same as the wings of other two coils. In order to facilitate a direct comparison, the parameters of the three coils, i.e., operating frequency, radius, number of turns, and impressed current, given in Table II, were taken from [47]. The analysis undertaken in [47] showed the maximum of the induced current normalized amplitude to occur at this frequency.

Contrary to the detailed geometrical coil model [32], the presented model does not account for the spacings between the multiple coil windings.

In all cases, the coils were placed over the primary motor cortex area, with a distance of 1 cm between surface of the brain and the geometric center of the coil. Since the actual coil geometry, i.e., the windings separation, the thickness of the coil insulation, as well as the casing, are neglected in this study, the chosen separation from the coil geometric center should be valid in this case. In case of a detailed coil model, the distance from the surface of the coil should be given.

A. Electric Field

The results obtained via the proposed model are compared to the analytical results obtained via (22) and (23). Calculated values for the maximum electric field are presented in Table III, while in Fig. 3, the induced electric field in coronal cross section is shown.

The comparison of the results shows that the distribution of the electric field in both cases is similar. Quantitatively, the results obtained via the proposed model show significantly lower values than the analytical ones, but this was expected, since the analytical method does not account for the electric field due to accumulation of charges. It is shown in [31] that the electric field

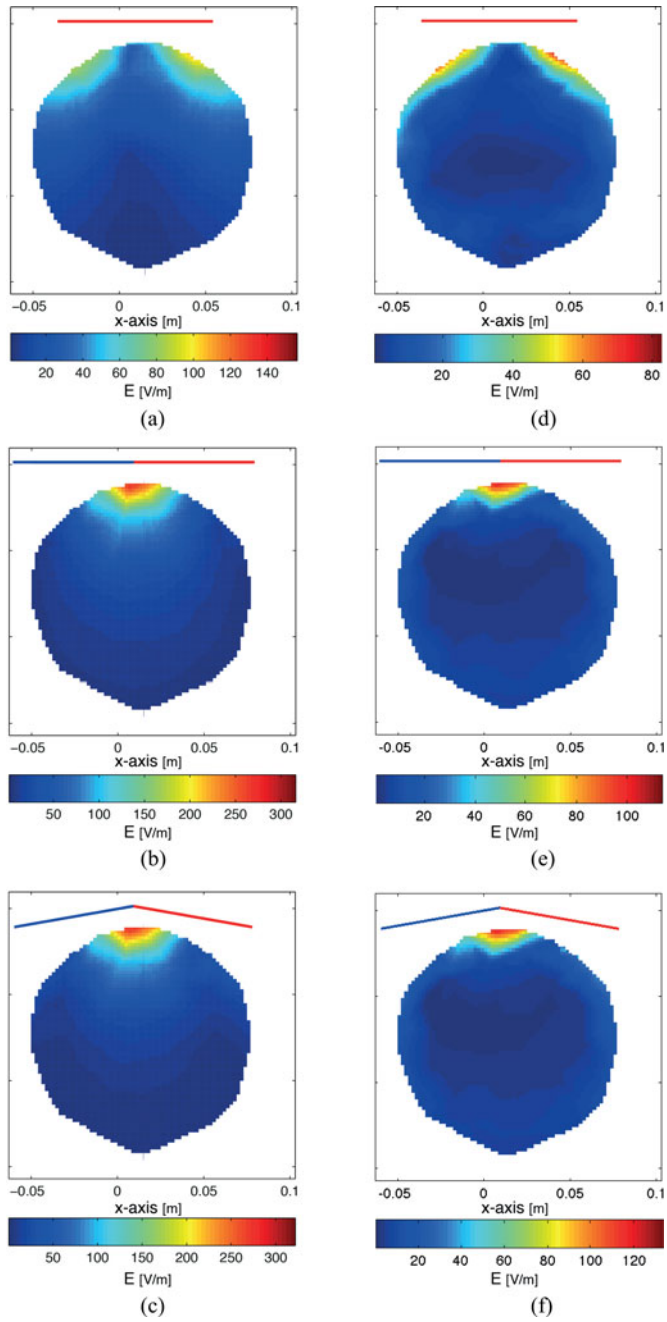

Fig. 3. Comparison of induced electric field in the human brain (coronal cross section). The results on the left are obtained via analytical expressions for the (a) circular, (b) 8-coil, and (c) butterfly coil, while the results on the right are obtained via proposed model for the (d) circular, (e) 8-coil, and (f) butterfly coil.

can decrease due to the shielding effect of the surface charges being accumulated at the surface.

Fig. 3 confirms the well-known fact that maximum electric field of the 8-coil is under the coil center, while for the circular coil, it is under the windings. Also, by tilting the windings of the 8-coil by as much as 10°, as it is the case for the used butterfly coil, a higher value of the electric field is obtained. Fig. 4 shows the calculated electric field at the brain surface in greater detail.

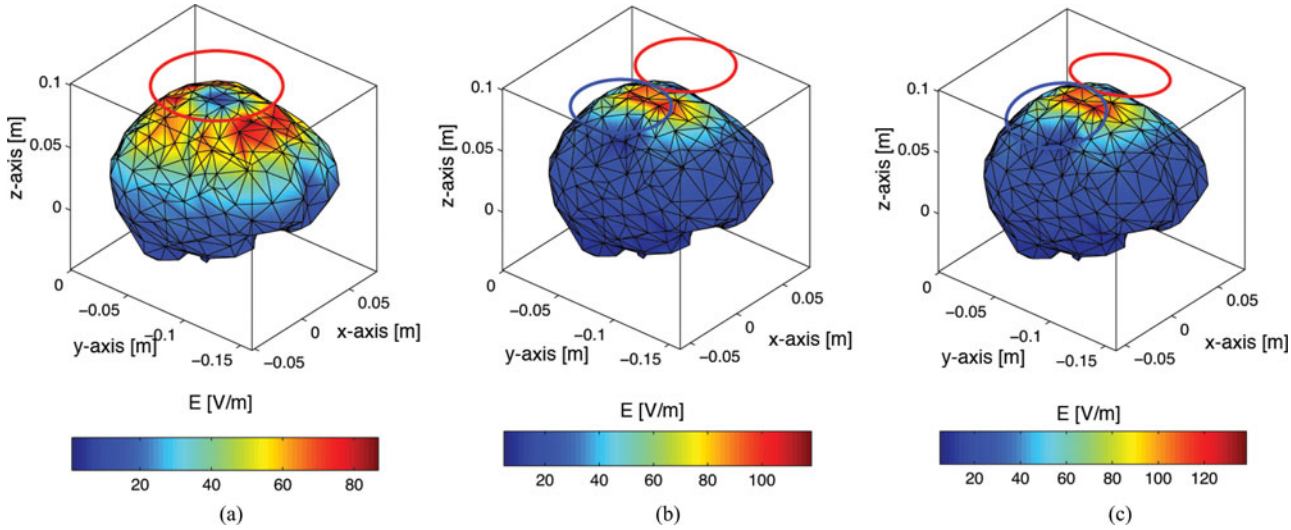

Fig. 4. Induced electric field on the brain surface due to: (a) Circular coil, (b) 8-coil, and (c) butterfly coil. All coils are placed 1 cm over the primary motor cortex.

TABLE IV
COMPARISON OF THE MAXIMUM VALUE OF INDUCED ELECTRIC CURRENT

		Circular	8-coil	Butterfly
E_{max}	[V/m]	86.8302	118.2815	138.4188
$J_{max,ind}$	[A/m^2]	7.483	10.194	11.929

TABLE V
COMPARISON OF MAXIMUM MAGNETIC FLUX DENSITY OBTAINED VIA ANALYTICAL EXPRESSION AND VIA PROPOSED MODEL

		Circular	8-coil	Butterfly
		Analytical		
B_{max}	[T]	0.679	0.672	0.826
		Proposed SIE model		
B_{max}	[T]	0.750	0.656	0.792

B. Current Density

From distribution of the electric field inside the brain, the induced current density J can be obtained using (26). The results for the maximum electric current density $J_{max,ind}$, for the homogeneous brain model, are given in Table IV.

The obtained current density value for the first coil is comparable to the results reported in [47], where a circular coil of similar parameters was used, but on a four tissue brain model. Kowalski *et al.* [47] determined the current density threshold value of 6 A/m^2 for the excitation of motor cortex area, while the proposed model in this paper obtained maximum value of 7.483 A/m^2.

C. Magnetic Flux Density

Finally, the results for the magnetic flux density, calculated by using (20) and (25), are compared to the analytical results. The obtained results for the maximum values are given in Table V, while Fig. 5 shows comparison of the magnetic flux density in the coronal cross section. The results indicate that the presence of the brain does not significantly disturb the magnetic field of the coil, although a lower maximum value of the magnetic flux density was obtained for the 8-coil and butterfly coil. The coronal distribution of the magnetic flux density obtained using the proposed SIE model shows some discontinuities. This is related to the interpolation method used. Namely, the magnetic field obtained via (20) is calculated at the discrete points in the brain from which the value at neighboring area is determined by the interpolation. This numerical artifact could be overcome by determining the field at more finer resolution. The distribution of the magnetic flux density B on the surface of the brain is presented in more detail in Fig. 6.

As a final comparison between the results for three coils calculated by the proposed SIE-based method of this study, the Fig. 7 can be used, where the dependence of the induced electric field E and magnetic flux density B on the distance from the brain surface is shown. From Fig. 7, the rapid decrease of both E and B under the geometric center of the brain is clearly evident. The increase in the amplitude seen at the bottom of the brain is due to the vicinity of these points, where the field is calculated to the source point on the ventral brain surface. This is known in computational electromagnetics as the near singularity. The solution is to increase the number of integration points or to carefully choose the place of the integration points.

IV. DISCUSSION

Some of the limitations of the present model should be addressed at this point. The homogeneous brain model insulated in the free space does not represent a realistic scenario. The actual brain is surrounded by various tissues such as e.g., cerebrospinal fluid (CSF), adipose, skull, and scalp. The presence of these tissues will affect the overall distribution of the fields as well as induced current densities. Although the analysis in [48]

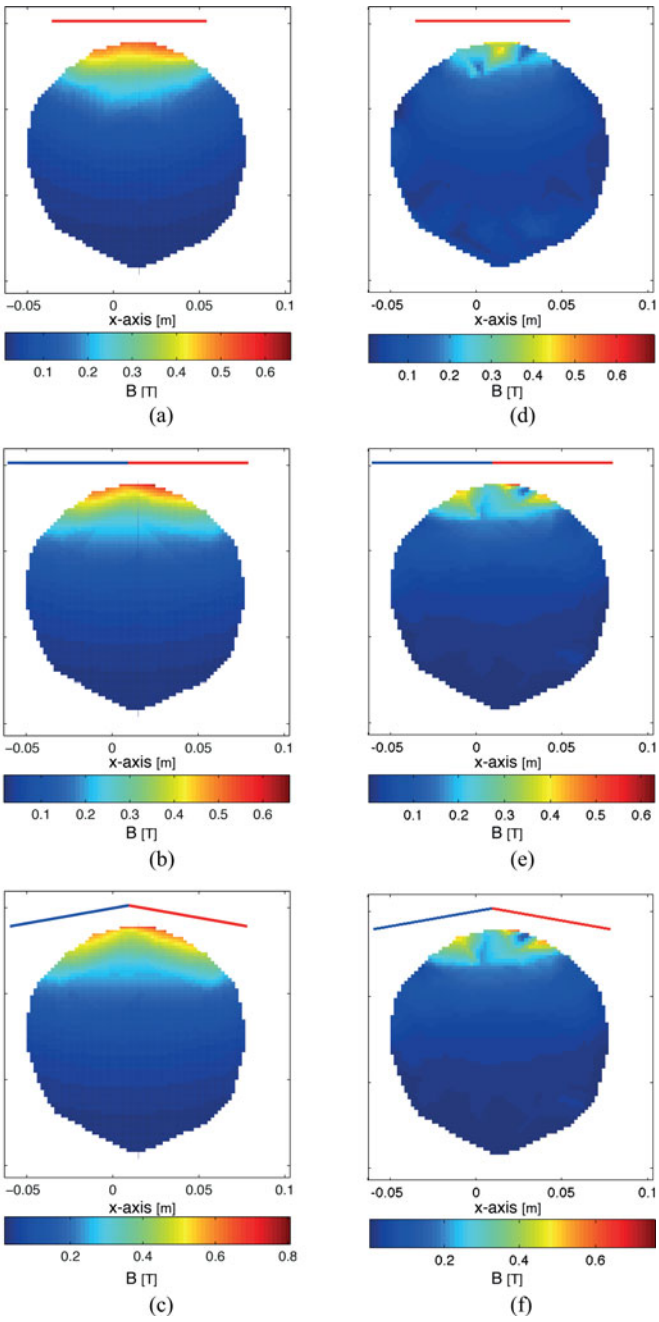

Fig. 5. Comparison of magnetic flux density in the human brain (coronal cross section). The results on the left are obtained via analytical expressions for the (a) circular, (b) 8-coil, and (c) butterfly coil, while the results on the right are obtained via proposed model for the (d) circular, (e) 8-coil, and (f) butterfly coil.

showed that the inclusion of the skull or CSF would not affect the distribution of currents in the adjacent cortex of the brain, other models showed the contrary [31], hence, an additional verification using the integral equation-based formulation could be beneficial. The future work should therefore be related to the inclusion of the surrounding tissues such as skull and scalp.

Another important thing to consider is the heterogeneity of the actual brain. The presented paper uses properties of the single homogeneous tissue whose value is given as the average between the WM and the GM. Given that WM and GM properties differ,

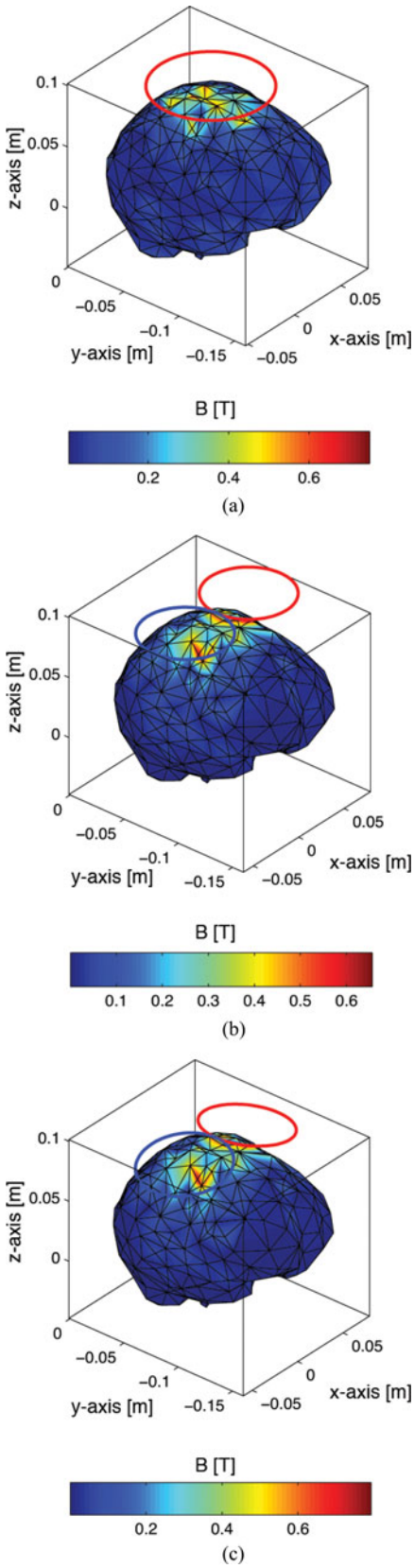

Fig. 6. Magnetic flux density on the brain surface due to: (a) Circular coil, (b) 8-coil, and (c) butterfly coil. All coils are placed 1 cm over the primary motor cortex.

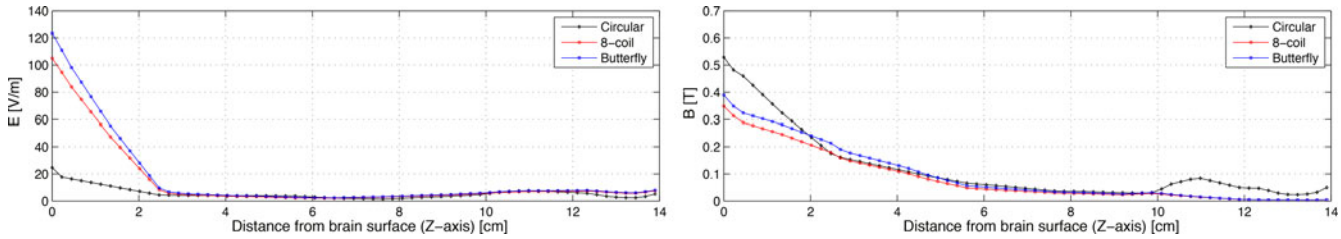

Fig. 7. Dependence of induced electric field E and magnetic flux density B on the distance from the brain surface. The values given are on the points directly under the coil geometric center.

one may expect the induced electric field values to increase or decrease at the boundaries between different tissues [31].

The brain surface model presented in this paper is smoothed out neglecting the detailed structures such as gyri and sulci. The proposed SIE formulation is applicable to an arbitrarily-shaped biological tissue, including a more detailed brain model taking the cortex foldings into account. The downside of the detailed description of the brain is the total number of elements required to accurately represent the geometry. This would consequently lead to a very large matrix system (18) whose solution would require the use of advanced techniques such as multilevel fast multipole method [49].

In addition to the detailed brain model, a more detailed description of the stimulating coil is also necessary, in order to give more accurate results. The simple description of the actual TMS coil is used in this paper, neglecting the separation between coil windings, the thickness of the coil insulation, and the casing. The model developed in [32] could be used to improve on the coil description.

V. Conclusion

This paper deals with the SIE-based model for TMS. The formulation is based on the coupled set of integral equations for the electric field. The corresponding SIE set is handled by a MoM scheme. The developed model takes into account the inductive and capacitive effects via the parameters of a homogeneous brain tissue, as well as propagation effects, often being neglected when quasi-static approximation is used. The numerical results obtained for the induced electric field, current density, and magnetic flux density are in a good agreement with the analysis from [47] as well as to the results obtained by analytical approach. The future work will be related to the development of a more detailed geometrical model of the human brain, which will take into account complex cortical columnar structures, as well as some additional brain tissues.

Appendix A

Applying the vector identity

$$\nabla(\phi\psi) = \phi\nabla\psi + \psi\nabla\phi \tag{27}$$

on the second integral in (10), where ϕ and ψ are two arbitrary scalar functions, the integrand can be written as

$$\nabla\left[\nabla'_S \cdot \vec{J}(\vec{r}\,')G_n(\vec{r},\vec{r}\,')\right] = \nabla\left[\nabla'_S \cdot \vec{J}(\vec{r}\,')\right] G_n(\vec{r},\vec{r}\,') + \nabla'_S \cdot \vec{J}(\vec{r}\,')\nabla G_n(\vec{r},\vec{r}\,'). \tag{28}$$

The first term on the right-hand side of (28) is zero due to the fact that the surface gradient operator acts with respect to the observation point $\vec{r}$.

Similarly, applying the vector identity

$$\nabla \times (\phi\vec{A}) = \nabla\phi \times \vec{A} + \phi\nabla \times \vec{A} \tag{29}$$

on the third integral in (10), where $\vec{A}$ is arbitrary vector function, the integrand can be written as

$$\nabla \times \left[\vec{M}(\vec{r}\,')G_n(\vec{r},\vec{r}\,')\right] = G_n(\vec{r},\vec{r}\,')\nabla \times \vec{M}(\vec{r}\,') + \nabla G_n(\vec{r},\vec{r}\,') \times \vec{M}(\vec{r}\,') \tag{30}$$

where, again, the first term on the right-hand side of (30) vanishes due to the fact that curl operator acting on $\vec{M}(\vec{r}\,')$ is defined with respect to the observation point $\vec{r}$.

Using the property $\vec{A} \times \vec{B} = -\vec{B} \times \vec{A}$ of the vector product, as well as the property for the gradient of Green's function

$$\nabla G_n(\vec{r},\vec{r}\,') = -\nabla' G_n(\vec{r},\vec{r}\,') \tag{31}$$

one can obtain the expression (11).

Appendix B

Multiplying (11) by the set of a test functions $\vec{f}_m$, where $\vec{f}_m = \vec{f}_n$, and integrating over surface S, yields

$$\begin{aligned} &j\omega\mu_i \sum_{n=1}^{N} J_n \iint_S \vec{f}_m(\vec{r}) \cdot \iint_{S'} \vec{f}_n(\vec{r}\,')G_i(\vec{r},\vec{r}\,')\,dS'\,dS \\ &- \frac{j}{\omega\varepsilon_i}\sum_{n=1}^{N} J_n \iint_S \vec{f}_m(\vec{r}) \cdot \iint_{S'} \nabla'_S \cdot \vec{f}_n(\vec{r}\,')\nabla G_i(\vec{r},\vec{r}\,')\,dS'dS \\ &+ \sum_{n=1}^{N} M_n \iint_S \vec{f}_m(\vec{r}) \cdot \iint_{S'} \vec{g}_n(\vec{r}\,') \times \nabla' G_i(\vec{r},\vec{r}\,')\,dS'dS \\ &= \begin{cases} \iint_S \vec{f}_m(\vec{r}) \cdot \vec{E}^{\text{inc}}\,dS, & i = 1 \\ 0, & i = 2 \end{cases} \end{aligned} \tag{32}$$

where i represents the index of the medium.

From the second term of (32), the gradient operator acting on the Green's function can be transferred to the test function. Reversing the order of integration in the double surface integral leads to

$$\iint_{S'} \nabla'_S \cdot \vec{f}_n(\vec{r}\,') \iint_S \vec{f}_m(\vec{r}) \cdot \nabla G_i(\vec{r},\vec{r}\,')\,dS\,dS'. \tag{33}$$

Using the vector identity

$$\nabla \cdot (\phi \vec{A}) = \vec{A} \cdot \nabla \phi + \phi \nabla \cdot \vec{A} \tag{34}$$

enables one to rewrite the inner integral of (33) as

$$\iint_S \vec{f}_m(\vec{r}) \cdot \nabla G_i(\vec{r}, \vec{r}')\, dS = \iint_S \nabla_S \cdot (\vec{f}_m(\vec{r}) G_i(\vec{r}, \vec{r}'))\, dS - \iint_S G_i(\vec{r}, \vec{r}') \nabla_S \cdot \vec{f}_m(\vec{r})\, dS \tag{35}$$

where ∇_S is the surface divergence operator.

Next, the surface divergence theorem can be applied on the first right-hand side term of (35), transferring the surface integral to the boundary integral. Using the definition of the RWG function (14), one can easily show that this boundary integral vanishes

$$\iint_S \nabla_S \cdot (\vec{f}_m(\vec{r}) G_i(\vec{r}, \vec{r}'))\, dS = \oint_c (\vec{f}_m(\vec{r}) G_i(\vec{r}, \vec{r}')) \cdot \hat{u}\, dl = 0 \tag{36}$$

leaving only the second term of (35). In (36), the normal on the boundary is represented by $\hat{u}$.

After rearranging, the double surface integral from (33) can be written as

$$-\iint_S \nabla_S \cdot \vec{f}_m(\vec{r}) \iint_{S'} \nabla'_S \cdot \vec{f}_n(\vec{r}') G_i(\vec{r}, \vec{r}')\, dS'\, dS. \tag{37}$$

The last term from the left-hand side of (32) is a bit trickier. In the limiting case when $R \to 0$, i.e., when the observation point $\vec{r}$ is near the source point $\vec{r}'$, this integral becomes hypersingular, while the other two integrals become singular. It could be shown that in the limiting case $R \to 0$, the latter ones vanish, while for the former one, it is not the case.

Therefore, one needs to exclude very small hemispherical region around the source point on surface S and determine the residual value of this integral on it. The integration domain S is hence split in two parts, the excluded part δ and the original part reduced by δ, i.e., $S - \delta$.

Separating the third integral from (11) in this way

$$\iint_S \vec{M}(\vec{r}') \times \nabla' G(\vec{r}, \vec{r}')\, dS' = \iint_{S-\delta} [\ldots]\, dS' + \iint_\delta [\ldots]\, dS' \tag{38}$$

the limiting case value can be determined

$$\begin{aligned}
&\lim_{R\to 0} \iint_\delta \vec{M}(\vec{r}') \times \nabla' G(\vec{r}, \vec{r}')\, dS' \\
&= \lim_{R\to 0} \iint_\delta \vec{M}(\vec{r}') \times \hat{R}(1 + jkR) \frac{e^{-jkR}}{4\pi R^2} \varepsilon^2 \sin\theta\, d\theta\, d\varphi \\
&= \frac{1}{4\pi} \int_0^{2\pi} \int_0^{\frac{\pi}{2}} \vec{M}(\vec{r}') \times \hat{R} \sin\theta\, d\theta\, d\varphi \\
&= \frac{1}{4\pi} 2\pi \int_0^{\frac{\pi}{2}} \vec{M}(\vec{r}') \times \hat{R} \sin\theta\, d\theta \\
&= \pm \frac{1}{2} \hat{n} \times \vec{M}(\vec{r}').
\end{aligned} \tag{39}$$

The sign in (39) depends from which side the observation point is approaching the source point on S. If the observation point is in medium 1, the sign is positive, otherwise it is negative.

Inserting (39) into (38), it leads to the integral equation set (16).

REFERENCES

[1] E. Wassermann *et al.*, Eds., *Oxford Handbook of Transcranial Stimulation*, 1st ed. New York, NY, USA: Oxford Univ. Press, 2008.

[2] A. Pascual-Leone *et al.*, Eds., *Handbook of Transcranial Magnetic Stimulation*, 1st ed. London, U.K.: Hodder Arnold, 2002.

[3] M. Hallett, "Transcranial magnetic stimulation and the human brain," *Nature*, vol. 406, no. 6792, pp. 147–150, 2000.

[4] R. Plonsey and R. C. Barr, *Bioelectricity: A Quantitative Approach*, 3rd ed. New York, NY, USA: Springer, 2007.

[5] A. T. Barker *et al.*, "Non-invasive magnetic stimulation of the human motor cortex," *Lancet*, vol. 1, pp. 1106–1107, 1985.

[6] S. Ueno *et al.*, "Localized stimulation of neural tissues in the brain by means of a paired configuration of time varying magnetic fields," *J. Appl. Phys.*, vol. 64, no. 10, pp. 5862–5864, 1988.

[7] S. Ueno *et al.*, "Functional mapping of the human motor cortex obtained by focal and vectorial magnetic stimulation of the brain," *IEEE Trans. Magn.*, vol. 26, no. 5, pp. 1539–1544, Sep. 1990.

[8] J. Ruohonen and R. J. Ilmoniemi, "Focusing and targeting of magnetic brain stimulation using multiple coils," *Med. Biol. Eng. Comput.*, vol. 36, no. 3, pp. 297–301, 1998.

[9] J. Ruohonen *et al.*, "Theory of multichannel magnetic stimulation: Toward functional neuromuscular rehabilitation," *IEEE Trans. Biomed. Eng.*, vol. 46, no. 6, pp. 646–651, Jun. 1999.

[10] L. Gomez *et al.*, "Numerical analysis and design of single-source multicoil TMS for deep and focused brain stimulation," *IEEE Trans. Biomed. Eng.*, vol. 60, no. 10, pp. 2771–2782, Oct. 2013.

[11] F. Grandori and P. Ravazzani, "Magnetic stimulation of the motor cortex-theoretical considerations," *IEEE Trans. Biomed. Eng.*, vol. 38, no. 2, pp. 180–191, Feb. 1991.

[12] N. M. Branston and P. S. Tofts, "Analysis of the distribution of currents induced by a changing magnetic field in a volume conductor," *Phys. Med. Biol.*, vol. 36, no. 2, pp. 161–168, 1991.

[13] M. Nadeem *et al.*, "Computation of electric and magnetic stimulation in human head using the 3-D impedance method," *IEEE Trans. Biomed. Eng.*, vol. 50, no. 7, pp. 900–907, Jul. 2003.

[14] F. S. Salinas *et al.*, "3D modeling of the total electric field induced by transcranial magnetic stimulation using the boundary element method," *Phys. Med. Biol.*, vol. 54, pp. 3631–3647, 2009.

[15] M. Chen and D. J. Mogul, "Using increased structural detail of the cortex to improve the accuracy of modeling the effects of transcranial magnetic stimulation on neocortical activation," *IEEE Trans. Biomed. Eng.*, vol. 57, no. 5, pp. 1216–1226, May 2010.

[16] H. Eaton, "Electric field induced in a spherical volume conductor from arbitrary coils: Application to magnetic stimulation and MEG," *Med. Biol. Eng. Comput.*, vol. 30, no. 4, pp. 433–440, 1992.

[17] W. C. Chew *et al.*, *Integral Equation Methods for Electromagnetic and Elastic Waves*. San Rafael, CA, USA: Morgan & Claypol, 2009.

[18] A. Nummenmaa *et al.*. (2013, Oct.). Comparison of spherical and realistically shaped boundary element head models for transcranial magnetic stimulation navigation. *Clin. Neurophysiol.* [Online]. *124(10)*, pp. 1995–2007. Available: http://dx.doi.org/10.1016/j.clinph.2013.04.019

[19] R. Plonsey and D. B. Heppner, "Considerations of quasi-stationarity in electrophysiological systems," *Bull. Math. Biol.*, vol. 29, no. 4, pp. 657–664, 1967.

[20] T. Wagner *et al.*, "Three-dimensional head model simulation of transcranial magnetic stimulation," *IEEE Trans. Biomed. Eng.*, vol. 51, no. 9, pp. 1586–1598, Sep. 2004.

[21] C. Gabriel *et al.*, "The dielectric properties of biological tissues: I. Literature survey," *Phys. Med. Biol.*, vol. 41, pp. 2231–2248, 1996.

[22] S. Gabriel *et al.*, "The dielectric properties of biological tissues: III. Parametric models for the dielectric spectrum of tissues," *Phys. Med. Biol.*, vol. 41, pp. 2271–2293, 1996.

[23] N. S. Stoykov *et al.*, "Frequency- and time-domain FEM models of EMG: Capacitive effects and aspects of dispersion," *IEEE Trans. Biomed. Eng.*, vol. 49, no. 8, pp. 763–772, Aug. 2002.

[24] C. Butson and C. C. McIntyre, "Tissue and electrode capacitance reduce neural activation volumes during deep brain stimulation," *Clin. Neurophysiol.*, vol. 116, no. 10, pp. 2490–2500, 2005.
[25] B. Tracey and M. Williams, "Computationally efficient bioelectric field modeling and effects of frequency-dependent tissue capacitance," *J. Neural Eng.*, vol. 8, pp. 1–7, 2011.
[26] C. A. Bossetti *et al.*, "Analysis of the quasi-static approximation for calculating potentials generated by neural stimulation," *J. Neural Eng.*, vol. 5, pp. 44–53, 2008.
[27] P. Tofts, "The distribution of induced currents in magnetic stimulation of the nervous system," *Phys. Med. Biol.*, vol. 35, no. 8, pp. 1119–1128, 1990.
[28] K. R. Davey *et al.*, "Prediction of magnetically induced electric fields in biological tissue," *IEEE Trans. Biomed. Eng.*, vol. 38, no. 5, pp. 418–422, May 1991.
[29] P. Ravazzani *et al.*, "Magnetic stimulation of the nervous system: Induced electric field in unbounded, semi-infinite, spherical, and cylindrical media," *Ann. Biomed. Eng.*, vol. 24, no. 5, pp. 606–616, 1996.
[30] J. Starzynski *et al.*, "Simulation of magnetic stimulation of the brain," *IEEE Trans. Magn.*, vol. 38, no. 2, pp. 1237–1240, Mar. 2002.
[31] P. C. Miranda *et al.*, "The electric field induced in the brain by magnetic stimulation: A 3-D finite-element analysis of the effect of tissue heterogeneity and anisotropy," *IEEE Trans. Biomed. Eng.*, vol. 50, no. 9, pp. 1074–1085, Sep. 2003.
[32] F. S. Salinas *et al.*, "Detailed 3D models of the induced electric field of transcranial magnetic stimulation coils," *Phys. Med. Biol.*, vol. 52, pp. 2879–2892, 2007.
[33] N. De Geeter *et al.*, "An efficient 3-D eddy-current solver using an independent impedance method for transcranial magnetic stimulation," *IEEE Trans. Biomed. Eng.*, vol. 58, no. 2, pp. 310–320, Feb. 2011.
[34] M. Stenroos *et al.* (2014, Mar.). Comparison of three-shell and simplified volume conductor models in magnetoencephalography. *NeuroImage* [Online]. pp. 1–12. Available: http://dx.doi.org/10.1016/j.neuroimage.2014.01.006
[35] R. Harrington, "Boundary integral formulations for homogeneous material bodies," *J. Electromagn. Waves Appl.*, vol. 3, no. 1, pp. 1–15, 1989.
[36] A. J. Poggio and E. K. Miller, "Integral equation solutions of three–dimensional scattering problems," in *Computer Techniques for Electromagnetics*, 2nd ed., R. Mittra, Ed. Bristol, PA, USA: Hemisphere, 1987, ch. 4, pp. 159–264.
[37] K. Umashankar *et al.*, "Electromagnetic scattering by arbitrary shaped three-dimensional homogeneous lossy dielectric objects," *IEEE Trans. Antennas Propagation*, vol. 34, no. 6, pp. 758–766, Jun. 1986.
[38] S. M. Blinkov and I. I. Glezer, *The Human Brain in Figures and Tables. A Quantitative Handbook*. New York, NY, USA: Plenum, 1968.
[39] P. Cignoni *et al.*, "Meshlab: an opensource mesh processing tool," *in Proc. IEEE Eurographics Italian Chapter Conf.*, pp. 129–136, 2008.
[40] S. Rao *et al.*, "Electromagnetic scattering by surfaces of arbitrary shape," *IEEE Trans. Antennas Propag.*, vol. 30, no. 3, pp. 409–418, May 1982.
[41] B. J. Roth *et al.*, "A theoretical calculation of the electric field induced in the cortex during magnetic stimulation," *Electroencephalography Clin. Neurophysiol.*, vol. 81, no. 1, pp. 47–56, 1991.
[42] L. G. Cohen *et al.*, "Effects of coil design on delivery of focal magnetic stimulation. Technical considerations," *Electroencephalography Clin. Neurophysiol.*, vol. 75, no. 4, pp. 350–357, 1990.
[43] C. Gabriel and S. Gabriel, "Compilation of the dielectric properties of body tissues at RF and microwave frequencies," King's College London, London, U.K., Tech. Rep. AL/OE-TR-1996-0037, 1996.
[44] S. Gabriel *et al.* (1996, Nov.). The dielectric properties of biological tissues: II. Measurements in the frequency range 10 Hz to 20 GHz. *Phys. Med. Biol.* [Online]. *41(11)*, pp. 2251–2269. Available: http://stacks.iop.org/0031-9155/41/i=11/a=002
[45] S. B. Baumann *et al.*, "The electrical conductivity of human cerebrospinal fluid at body temperature," *Bioelectromagnetics*, vol. 44, no. 3, pp. 220–223, 1997.
[46] C. Gabriel *et al.*. (2009, Aug.). Electrical conductivity of tissue at frequencies below 1 MHz. *Physics Med. Biol.* [Online]. 54(16), p. 4863. Available: http://stacks.iop.org/0031-9155/54/i=16/a=002
[47] T. Kowalski *et al.*, "Current density threshold for the stimulation of neurons in the motor cortex area," *Bioelectromagnetics*, vol. 23, no. 6, pp. 421–428, 2002.
[48] L. Golestanirad *et al.*, "Effect of the model accuracy on the result of computed current densities in the simulation of transcranial magnetic stimulation," *IEEE Trans. Magn.*, vol. 46, no. 12, pp. 4046–4051, Dec. 2010.
[49] V. Rokhlin, "Rapid solution of integral equations of classic potential theory," *J. Comput. Phys.*, vol. 60, no. 2, pp. 187–207, 1985.

Authors' photographs and biographies not available at the time of publication.